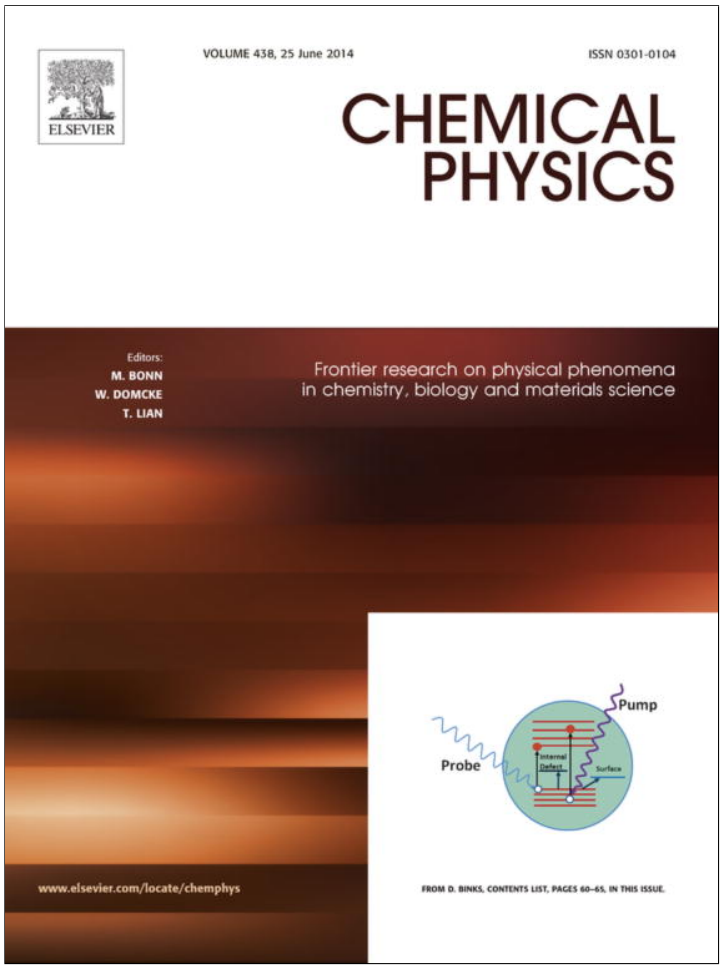

Chemical Physics 438 (2014) 16–22

Contents lists available at ScienceDirect

Chemical Physics

journal homepage: www.elsevier.com/locate/chemphys

Study of atomic and molecular oxygen chemisorption on BC_3 nanotubes with Stone–Wales defects using density functional theory

Seifollah Jalili [a,b,*], Elaheh Hosseinzadeh [a], Jeremy Schofield [c]

[a] Department of Chemistry, K.N. Toosi University of Technology, P.O. Box 15875-4416, Tehran, Iran
[b] Computational Physical Sciences Research Laboratory, School of Nano-Science, Institute for Research in Fundamental Sciences (IPM), P.O. Box 19395-5531, Tehran, Iran
[c] Chemical Physics Theory Group, Department of Chemistry, University of Toronto, 80 Saint George Street, Toronto, Ontario M5S 3H6, Canada

ARTICLE INFO

Article history:
Received 14 January 2014
In final form 23 April 2014
Available online 2 May 2014

Keywords:
Electronic band structure
Density of states
Functionalization
Reactivity
Half-metallic anti-ferromagnet

ABSTRACT

Density functional theory calculations are used to study the adsorption of chemical species including oxygen atom and oxygen molecule on the perfect and defective BC_3 nanotubes. Stone–Wales topological defects with four different bond rotations have been examined. The adsorption of atomic oxygen is exothermic in all cases, while for the molecular oxygen, some sites showed endothermic adsorption. Comparative studies on the adsorption of these chemical species shows the maintenance of semiconductive behavior of nanotubes, except for one of the systems, the defected nanotube with a circumferential C–C bond rotation. In this system, the adsorption of molecular oxygen generates a half-metallic antiferromagnet. The results obtained in this paper are relevant for chemical sensing and spintronics applications.

1. Introduction

The study of adsorption of different chemical species on the surface of carbon nanotubes (CNTs) has drawn considerable amount of attention due to the large surface to mass ratio and capability of these nanotubes as chemical sensors [1,2]. Nevertheless, the electronic properties of carbon nanotubes depend on the twist angle and diameter of the corresponding rolled graphene sheet. In addition, controlling the chirality of carbon nanotubes during their synthesis process is still demanding. One of the possible ways to modify the electronic properties of these nanotubes is to dope them with electron donors and accepters. Since the atomic radius of boron is close to that of carbon, it acts as an impurifier for CNTs [3,4]. Experimental and theoretical studies show that BC_3 nanodomains can be formed in a one-dimensional nanotube structure upon boron doping in CNTs and BC_3 nanotubes can be formed with relative stabilities comparable to those of CNTs [5]. BC_3 heteronanotubes contain C–C and B–C bonds but do not have any unstable B–B bond; hence these structures are stable [6]. Unlike CNTs, these nanotubes show electronic properties which do not depend on the diameter and chirality of the nanotubes. However, synthesized BC_3 nanotubes in the laboratory may have some imperfections [7]. The electronic structure of these electron-deficient NTs can be influenced by some defects such as vacancy defects and topological defects including Stone–Wales (SW) defects, which are obtained by rotation of a chemical bond by 90° [8].

The chemical reactivity of SW defects in CNTs has been investigated using density functional theory (DFT) calculations [9–11]. Although the structures of SW defects are demonstrated to be more active than those of the detect-free nanotubes in most previous works [12,13], Lu et al. showed that the reactivity of the central C–C bond of a SW defect in an armchair nanotube of (5,5) chirality with seven layers is less than that of a detect-free NT. This is thought to be due to the reduced pyramidalization angle (θ_p) of carbon atoms [14]. In another study on (5,5) carbon nanotubes, Bettinger showed that the enhanced reactivity of tubes with SW defects is introduced at C–C junctions other that the 7, 7 junction [15].

In contrast to carbon nanotubes with only nonpolar C–C bonds, BC_3 nanotubes are composed of BC bonds and have electron-deficient structures because boron has a lower electronegativity than carbon and hence the distribution of electron density around boron is much less than that around carbon [16]. Compared to CNTs, BC_3 nanotubes have different structural and electronic features. In this context, we focus on the adsorption features of perfect and defected BC_3 nanotubes.

In the present work, the adsorption of oxygen atom and oxygen molecule on the SW defects of BC_3 nanotubes are studied and geometrical and electronic changes as a result of the adsorption are investigated using DFT calculations. The obtained results are

* Corresponding author at: K.N. Toosi University of Technology, Department of Chemistry, Tehran, Iran. Tel.: +98 21 22853649; fax: +98 21 22853650.
E-mail address: sjalili@kntu.ac.ir (S. Jalili).

http://dx.doi.org/10.1016/j.chemphys.2014.04.010
0301-0104/

compared to those of detect-free BC_3 nanotubes. Similar studies have been carried out on carbon nanotubes [12–15]. So far, however, there has been little discussion about the chemical reactivity of SW defects in BC_3 nanotubes.

2. Computational methods

Density functional theory calculations were carried out using plane-wave basis set and ultrasoft pseudopotentials [17], implemented in the QUANTUM ESPRESSO package [18]. The generalized-gradient approximation (GGA) with the Perdew-Burke-Ernzerhof (PBE) functional [19] and a 360 eV cutoff for the plane-wave basis set was used in all computations.

Four unit cells of a (4,0) BC_3 nanotube were chosen along the tube axis and the tube was placed in a 20 Å × 20 Å × 17.08 Å supercell. Four types of Stone–Wales defects were created in the tube by rotating an axial or circumferential C–C or B–C bond. These defects are denoted by SW-CC-a, SW-CC-c, SW-BC-a, and SW-BC-c, as described in our previous work [8].

In order to investigate the reactivity, adsorbate species in different orientations were placed on top of different bonds or atoms of perfect and defected nanotubes, as shown in Fig. 1. The initial distance between the adsorbate and the sidewall of nanotubes were 1.2 Å. Geometries of the resulting BC_3 nanotubes with adsorbed species were optimized using the gamma point, with convergence thresholds of 0.001 meV in energy and 0.002 eV/Å in force. Binding (or adsorption) energies were evaluated as $E_{ads} = E[BC_3NT - adsorbate] - E[BC_3NT] - E[adsorbate]$, where E denotes the total energy of the optimized systems. A negative value for E_{ads} corresponds to exothermic adsorption. A $1 \times 1 \times 7$ grid of k-points generated by Monkhorst–Pack [20] scheme was used for the calculation of energy and other properties. For band structure calculations, 11 equally spaced k-points along the Γ–Z direction were used.

Optimized structures were also used to compute the average local ionization energy, $I(r)$, over grids covering both the inner and outer 0.001 a.u. surfaces of the defected nanotubes. $I(r)$ was calculated by the Multiwfn software [21], using the wave functions generated by Gaussian03 program [22] at PBEPBE/6-31G(d) level of theory. The generated Gaussian-type grid (.cube) files were plotted using VMD software [23].

3. Results and discussion

3.1. Electronic properties of defected BC_3 nanotubes

In order to study the effect of a SW defect on the electronic properties of BC_3 nanotubes, total density of states (TDOS) for perfect and defected tubes are calculated and plotted in Fig. 2. The perfect BC_3 nanotube is a semiconductor with a direct band gap of ~0.5 eV, in agreement with previous DFT calculations [6,24]. It has been observed by Picozzi, et al. that, after defect creation in the semiconducting single-walled carbon nanotubes, they remain to be semiconductors and only a slight reduction in the band gap occurs [25]. Similar results have been obtained for boron nitride nanotubes (BNNTs) [26]. Our results show that for BC_3 nanotubes, the Stone–Wales defects reduce the band gap, except for SW-BC-a system, for which the band gap does not change a lot. For perfect and defected tubes, the order of energy gap values is perfect ≈SW-BC-a > SW-CC-c > SW-BC-c > SW-CC-a.

For the SW-CC-a nanotube, as mentioned in our previous work [27], an acceptor state appears near the top of the valence band which causes this nanotube to have the lowest bad gap. The local

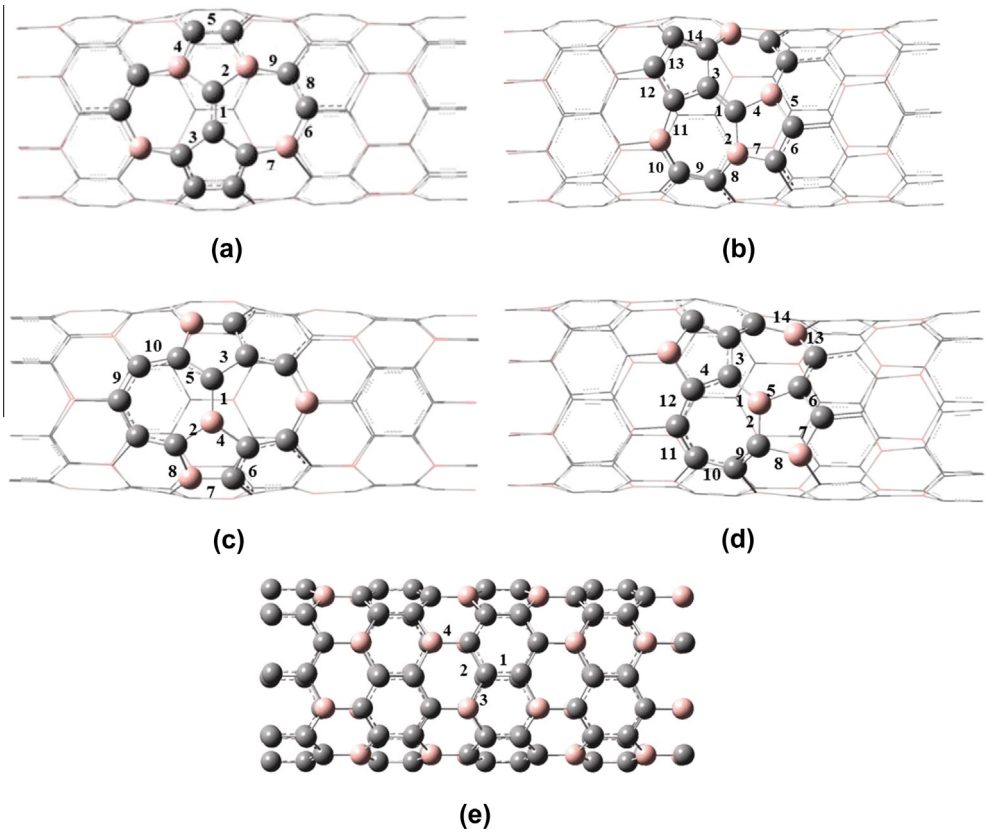

Fig. 1. Optimized geometries and adsorption sites for BC_3 nanotubes with a SW-CC-a (a), SW-CC-c (b), SW-BC-a (c), SW-BC-c (d) defect, along with a perfect BC_3 tube (e). Carbon and boron atoms are shown in grey and pink, respectively. (For interpretation of the references to color in this figure legend, the reader is referred to the web version of this article.)

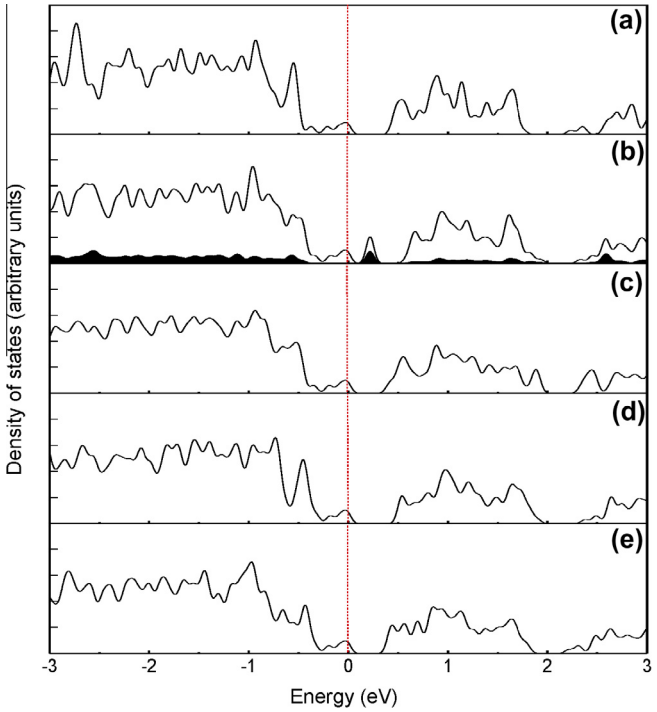

Fig. 2. Total density of states for perfect (a), SW-CC-a (b), SW-CC-c (c), SW-BC-a (d), and SW-BC-c (e) systems. The dotted line indicates the position of the Fermi energy. The local density of states for the central defect atoms and their first and second neighbors is also plotted in part (b).

density of states (LDOS) plot in Fig. 2(b) (the black curve with filled area under it) shows that this new state is mainly derived from the 2*p* atomic orbitals of central (rotated) atoms in SW defect and their first and second neighbors.

3.2. Chemical adsorption of atomic oxygen

Binding energies for atomic oxygen adsorption on different sites shown in Fig. 1 are listed in Table 1. In all cases, an oxygen atom which is initially placed above a carbon or boron atom migrates spontaneously to a neighboring B–C or C–C bridge position. For this reason, only the bridge sites are shown in Fig. 1 and Table 1. All the calculated binding energies are negative, i.e., the oxygen adsorption is exothermic in all cases. These results are in agreement with the studies of atomic oxygen adsorption on BNNTs with SW defects and on perfect CNTs [28,29].

Table 1
Binding energies (eV) for atomic oxygen adsorption on different sites in perfect and defective BC_3 nanotubes. Refer to Fig. 1 for site numberings.

Site	Perfect	SW-CC-a	SW-CC-c	SW-BC-a	SW-BC-c
1	−3.24	−4.21	−3.19	−5.82	−4.35
2	−3.99	−5.86	−5.75	−5.75	−5.83
3	−5.57	−4.74	−4.95	−4.81	−5.16
4	−4.44	−5.67	−5.50	−5.80	−3.67
5		−3.39	−6.08	−4.13	−4.90
6		−5.57	−4.68	−4.16	−4.16
7		−4.74	−5.15	−4.88	−6.23
8		−3.74	−4.93	−5.96	−5.23
9		−4.58	−2.85	−4.04	−3.68
10			−5.81	−3.22	−3.40
11			−6.33		−3.42
12			−4.07		−4.94
13			−5.28		−5.54
14			−3.92		−3.93

In a perfect BC_3 nanotube, oxygen chooses among possible binding sites in the order of 3 > 4 > 2 > 1 (refer to Fig. 1(e)). The most negative binding energy is obtained for a slanted B–C bond (site 3). B–C bonds are better than C–C bonds, and for each bond type, slanted bonds are preferred above axial bonds. For the BC_3 nanotubes with a SW defect, the adsorption on B–C bonds is still more exothermic than on C–C bonds, but a large number of different orientations are possible, which affect the binding of the oxygen atom. Note that the symmetry reduces the number of distinct adsorption sites, as it is clear for SW-CC-a and SW-BC-a systems.

The effect of orientation can be best understood by inspecting the binding energies for the adsorption on the 7–7 ring fusion (site 1) in defected nanotubes. The SW-BC-a tube shows the most exothermic binding on this site. The binding energy for this case (E_b = −5.82 eV) is more negative than all the values for a perfect tube. On the other hand, SW-CC-c tube shows the most endothermic adsorption on site 1, with a binding energy (E_b = −3.19 eV) that is even less negative than the perfect tube values. It is clear that for each bond type, B–C or C–C, the 7–7 junction is more reactive in the nanotubes with axial bond rotation. As we predicted before, the higher reactivity of the 7–7 junction for axial bond rotation is due to the higher pyramidalization angles for the two atoms forming this junction in BC_3 nanotubes [8].

The most stable configurations for the adsorption of an oxygen atom on perfect and defective BC_3 nanotubes are shown in Fig. 3. In all systems, the oxygen atom prefers a bridge site above a BC bond and forms two new bonds with boron and carbon atoms. As can be seen in Fig. 3, a distortion occurs upon the adsorption of oxygen on these nanotubes, resulting in the movement of boron and carbon atoms at adsorption site out of the nanotube surface and an increase in the underlying C–C and B–C bond lengths. This distortion is related to the *sp* [2] to *sp* [3] change of local hybridization of carbon and boron atoms.

As Fig. 3 and Table 1 show, the best adsorption site for the SW-CC-a tube is a on a B–C bond in 5–7 ring junction (site 2). For the other defective systems, this B–C bond is a 6–7 ring junction (site 11) for the SW-CC-c tube and a 5–6 ring junction for both SW-BC-a and SW-BC-c tubes (sites 8 and 7, respectively). For SW-CC-a, the most favorable position for the adsorption of oxygen (site 2) is in line with the fact that the underlying carbon and boron atoms have a significant contribution in the new defect state in band gap. A similar correlation has been observed for a carbon nanotube [9].

Compared to a perfect tube, the atomic oxygen adsorption for all these defected tubes are more exothermic, and the SW-CC-c system has the most negative binding energy among all of the systems studied. Since oxygen atom has a high electronegativity, these reactions involve charge transfer from the nanotube to the oxygen atom. The values of charge transferred in the most stable configurations for perfect, SW-CC-a, SW-CC-c, SW-BC-a, and SW-BC-c nanotubes are 0.33, 0.26, 0.27, 0.29, and 0.31 e, respectively.

Fig. 4 shows average local ionization energy, $\bar{I}(r)$ values of different positions on the surface of defected BC_3 nanotubes. These local minima are signs of the most active (less relaxed) positions of electrons and therefore, electrophilic or radical attacks on these sites are more favorable. $\bar{I}(r)$ is calculated from the following relation [30]

$$\bar{I}(r) = \frac{\sum_i \rho_i(r)|\varepsilon_i|}{\rho(r)}$$

where $\rho_i(r)$ and ε_i are the electron density function and orbital energy of the *i*-th molecular orbital, respectively. As Fig. 4 shows, the lowest value of $\bar{I}(r)$ (I_{min}) is related to the position with the most negative binding energy in all systems (see Table 1).

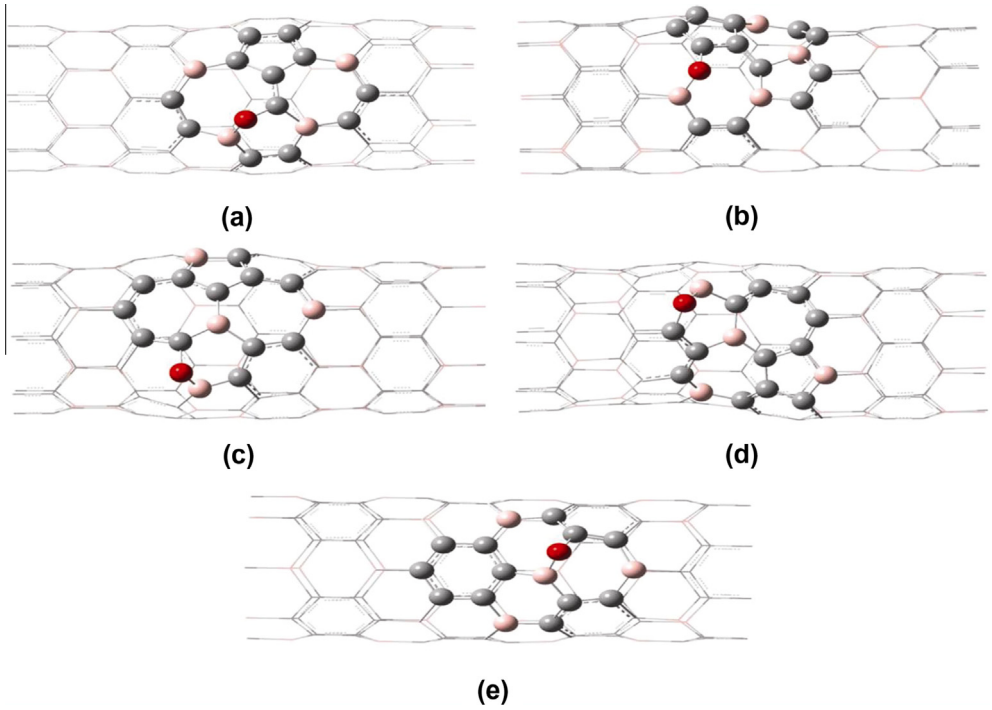

Fig. 3. Lowest-energy geometries for the chemisorption of atomic oxygen on SW-CC-a (a), SW-CC-c (b), SW-BC-a (c), SW-BC-c (d), and perfect (e) nanotubes.

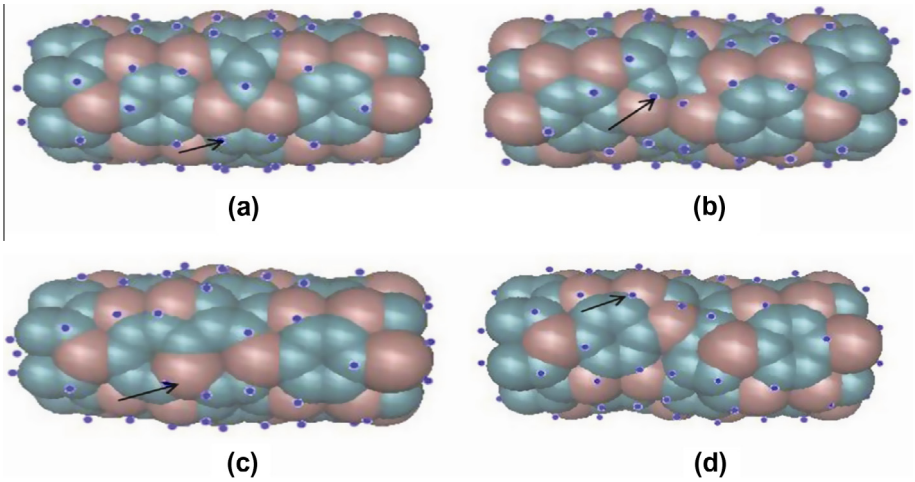

Fig. 4. Calculated averaged local ionization energies on the 0.001 a.u. surface of the SW-CC-a (a), SW-CC-c (b), SW-BC-a (c), SW-BC-c (d), and perfect (e) tubes. Green and pink spheres indicate carbon and boron atoms, respectively. Blue points show the points of I_{min} on the surfaces of nanotubes. The lowest value of I_{min} on the surface of nanotubes is indicated with a black arrow.

3.3. Chemical adsorption of molecular oxygen

The most stable configurations for the adsorption of an oxygen molecule on the perfect and defected BC_3 nanotubes are shown in Fig. 5. Similar to the atomic oxygen adsorption, O_2 molecule prefers the sites above B–C bonds. After the adsorption of an oxygen molecule, the B–C bond of the nanotube cleaves, new B–O and C–O bonds form and geometrical changes are appeared in nanotubes because of the significant interactions between O_2 and nanotubes. As Fig. 5 reveals, the oxygen bond cleavage does not occur in the adsorbed O_2 molecule on the SW-CC-a and perfect tubes. However, the bond length of O–O is greater than the O–O distance in a free O_2 molecule, for which the optimized bond length was found to be 1.203 Å. In these two systems, the O_2 bond is not parallel to the underlying bond in nanotube and oxygen adsorption leads to the formation of a distorted tetrahedron. Similar results are obtained for other defective BC_3 nanotubes, but the oxygen–oxygen bond cleaves in these systems. Overall, the O_2 molecule adsorption on BC_3 nanotubes is like a cycloaddition reaction.

The binding energies for molecular oxygen adsorption on perfect and defected BC_3 nanotubes are reported in Table 2 for the positions specified in Fig. 1. The first obvious feature in Table 2 is that the oxygen molecule adsorption for some positions is an endothermic process, while the binding energies in Table 1 for atomic oxygen adsorption were all negative. This is expected, because atomic oxygen is more reactive than the oxygen molecule. It was found in previous studies that the oxygen molecule adsorption on defect-free (8,0) BNNTs is endothermic (E_b = 1.60 eV) [28], whereas in the perfect BC_3 nanotubes, the chemical adsorption of molecular oxygen is exothermic in the most stable configuration

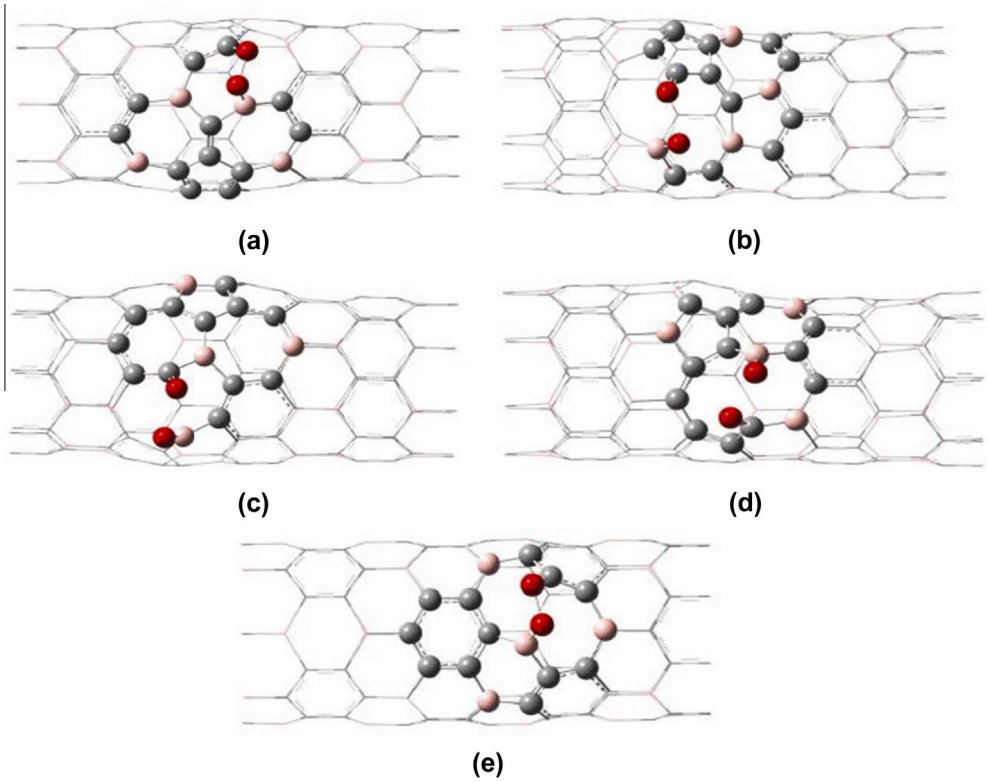

Fig. 5. Lowest-energy geometries for the chemisorption of molecular oxygen on SW-CC-a (a), SW-CC-c (b), SW-BC-a (c), SW-BC-c (d), and perfect (e) nanotubes.

Table 2
Binding energies (eV) for molecular oxygen adsorption on different sites in perfect and defective BC_3 nanotubes.

Site	Perfect	SW-CC-a	SW-CC-c	SW-BC-a	SW-BC-c
1	0.79	0.12	3.47	−1.42	−0.61
2	0.90	−1.89	−2.93	−0.86	−2.72
3	−2.27	0.79	1.59	1.24	−1.53
4	0.31	−1.97	−2.47	−0.89	1.37
5		0.57	−2.77	0.30	−1.47
6		−1.79	0.35	0.65	−1.27
7		−0.15	−0.66	−0.13	−2.67
8		0.77	−1.67	−2.37	−1.47
9		0.44	0.72	0.52	1.72
10			−2.68	0.73	0.87
11			−3.18		1.79
12			−0.06		−1.76
13			0.56		−2.13
14			−0.34		−0.09

(site 3, $E_b \approx -2.27$ eV). Moreover, for the adsorption on the 7–7 ring junction (site 1), the order of binding energies is similar to the atomic oxygen case. B–C bonds are preferred above C–C bonds and axial bond rotation is preferred above circumferential bond rotation.

The equilibrium structural parameters in the most stable configurations for molecular oxygen adsorption on perfect and defected BC_3 nanotubes are reported in Table 3. The structures with more negative binding energies have shorter B–O and C–O bonds and longer O–O bonds. The amount of the increase in the B–C bond length is also larger in these structures. Note that SW-CC-c/O_2 has the shortest C–O bond (typical of carbonyl) and the largest O–O and B–C distances, which implies the weakest through-space orbital interaction between B–O and C–O sites.

In a similar manner as atomic oxygen, the O_2 molecule adsorbs on BC_3 nanotubes with a charge transfer from nanotube to O_2. The

Table 3
Equilibrium structural parameters in the most stable configurations for the adsorption of O_2 on BC_3 nanotubes. d'_{BC} is the BC bond length (at the adsorption site) in a bare nanotube and d_{B-C}, d_{B-O}, d_{C-O}, and d_{O-O} show the different bond lengths after the oxygen adsorption.

Nanotube	d'_{B-C}	d_{B-C}	d_{B-O}	d_{C-O}	d_{O-O}
Perfect	1.54	2.65	1.39	1.36	1.52
SW-CC-a	1.55	2.51	1.42	1.36	1.50
SW-CC-c	1.56	3.06	1.32	1.24	2.10
SW-BC-a	1.55	2.64	1.30	1.25	2.07
SW-BC-c	1.50	2.82	1.31	1.24	2.02

values of charge transferred for the most stable configurations of perfect, SW-CC-a, SW-CC-c, SW-BC-a, and SW-BC-c nanotubes are 0.35, 0.37, 0.61, 0.59 and 0.64 e, respectively.

To study the effect of an adsorbed oxygen molecule on electronic properties of BC_3 nanotubes, electronic band structures, TDOS and LDOS (for O_2 and defect region atoms) plots were calculated. For perfect and SW-CC-a nanotubes, which adsorb the oxygen molecule without oxygen–oxygen bond cleavage, no significant change in electronic properties was observed after oxygen adsorption. The density of states plots for perfect/O_2 and SW-CC-a/O_2 systems are similar to Fig. 2(a) and (b), respectively. In addition, oxygen atoms do not contribute to any state around the Fermi level.

In the case of SW-BC-a and SW-BC-c, as Fig. 6 shows, oxygen adsorption alters the electronic band structures, but the semiconducting behavior is preserved in these systems. For SW-BC-a (Fig. 6(a)), two new states appear above and below the Fermi level, at the energies of ±0.3 eV. The new unoccupied state in the energy gap of SW-BC-a nanotube reduces the band gap from 0.40 eV to 0.15 eV. It has equal contributions from oxygen atoms and the atoms in the defect region of nanotube. The new occupied state

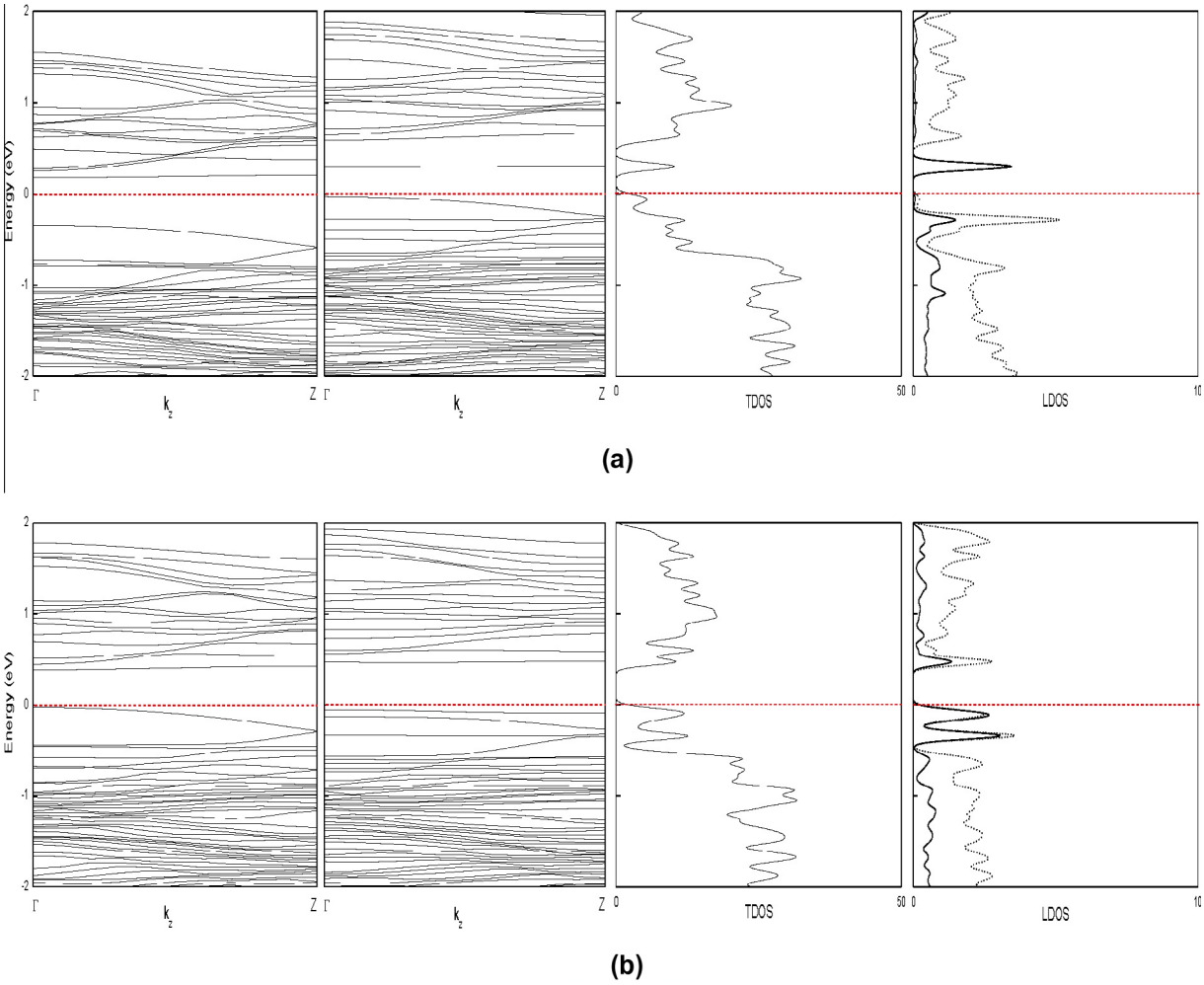

Fig. 6. Electronic properties for O_2 adsorption on SW-BC-a (a) and SW-BC-c (b) nanotubes. The panels from left to right are band structure of the bare tube, band structure and total density of states for the O_2-adsorbed tube, and local density of states plots for O_2 molecule (solid line) and its neighboring atoms in BC_3 tube (dotted line). Zero energy indicates the Fermi level.

in the valence band is mainly contributed by the defect region atoms of nanotube.

Fig. 6(b) shows that, upon oxygen molecule adsorption, two new bands are created below the Fermi level of SW-BC-c nanotube, at energies of −0.11 and −0.35 eV. They are derived from the 2*p* atomic orbitals of oxygen atoms and the atoms of nanotube at defect region. The band gap has been slightly (by ∼0.05 eV) increased in this case.

In all of the above cases, the nanotubes with a chemisorbed oxygen molecule have a zero magnetic moment, implying a spin-singlet state. The strong binding of chemisorbed oxygen would prefer a singlet state, since the electrons can be covalently paired in new bonds. Therefore, as oxygen molecule approaches the nanotube, its spin state changes from the ground state triplet to a singlet state. The observation of a singlet state in systems with oxygen chemisorption has been reported in many studies [29,31–34]. This change in spin state has been suggested as a rationale for the experimental observation of UV-light accelerated oxidation of CNTs, since UV light can excite the oxygen molecules to a higher energy singlet state, which reduces the energy barrier and leads to strong chemical bonds [35].

A totally different behavior is observed for the molecular oxygen adsorption on a BC_3 nanotube with a SW-CC-c defect. The net magnetic moment of the system is still zero, while its absolute value is 1.61 μ_B. Therefore, the SW-CC-c/O_2 system has an antiferromagnetic spin ordering. Fig. 7 shows the spin polarization for this system. Both σ and π electrons contribute to spin polarization. The spin-up and spin-down electrons are mainly accumulated around oxygen and nanotube atoms, respectively. The B–O moiety has a spin-unpaired electron and the ring carbon atoms neighboring the >C = O site have another spin-unpaired electron. This might be a source of antiferromagnetic spin-ordering in the SW-CC-c/O_2 system.

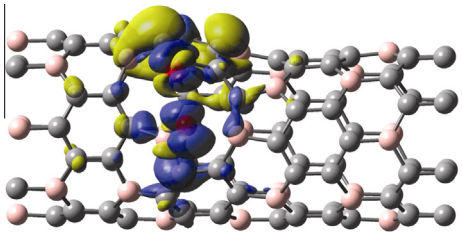

Fig. 7. Spin-density isosurfaces of SW-CC-c/ O_2 system for an isodensity value of 0.001 μ_B/Bohr [3]. Blue (dark) and yellow (light) regions correspond to positive and negative polarizations, respectively. (For interpretation of the references to color in this figure legend, the reader is referred to the web version of this article.)

Total and local DOS plots for the oxygen adsorption on a SW-CC-c nanotube are presented in Fig. 8. Inspection of the DOS plot

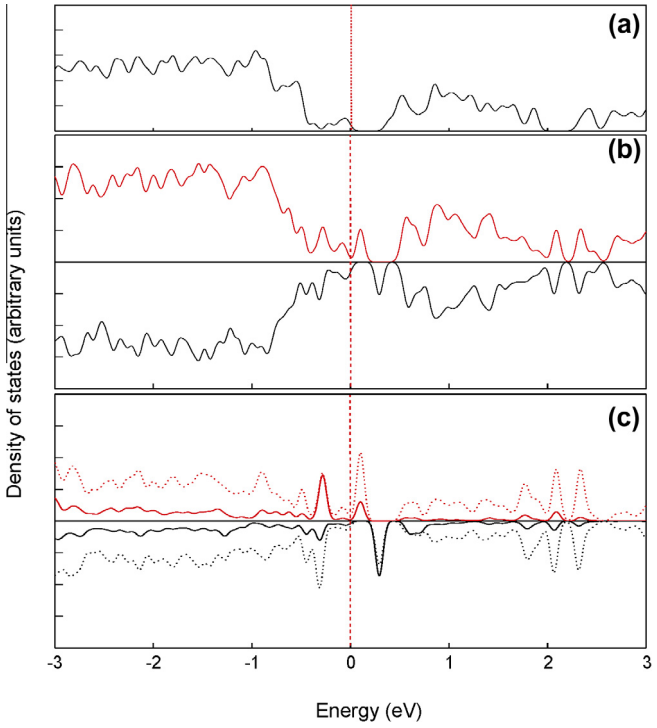

Fig. 8. Total density of states plots for a bare (a) and an O_2-adsorbed (b) SW-CC-c tube, and local density of states (c) for O_2 molecules (solid line) and its neighboring atoms in BC_3 tube (dotted line). For (b) and (c) parts, upper and lower panels are for spin-up and spin-down states, respectively. The Fermi level is at zero energy.

for the SW-cc-c/O_2 system in Fig. 8(b) shows that, compared to the bare tube (Fig. 8(a)), new spin-up and two spin-down states appear below and above the Fermi level. However, in contrast to conventional antiferromagnets, the TDOS curves in two spin directions are not identical. It seems that the vanishing net magnetic moment does not come from a symmetry relation between subsets of opposite spin or the presence of a spin-density wave. This situation can be occurred for a half-metallic antiferromagnet [36]. A finite value of DOS at Fermi level and the presence of an unoccupied state just above the Fermi level significantly improve the conductivity of the system for spin-up direction, while the system is a semiconductor in spin-down channel. The new vacant state above the Fermi level is spin-resolved. Therefore, the conduction electrons excited to these bands are completely spin-polarized, which is very important in spintronics applications [37].

LDOS plots in Fig. 8(c) show that the spin-up peak at the energy of −0.28 eV and the spin-down peak at 0.29 eV are equally contributed from the oxygen and nanotube atoms. In contrast, the spin-down state at −0.32 eV and the spin-up peak at 0.10 eV are mainly derived from the nanotube atoms in the defect region.

4. Conclusions

Concerning the reactivity of defect-free and SW-defected (4,0) BC_3 nanotubes, density functional theory calculations were employed to study the effect of O and O_2 chemical species adsorption. The results indicate that SW defect-region positions are more active than defect-free sites. The chemical adsorption of atomic oxygen on perfect and defective BC_3 nanotubes leads to epoxide formation. Comparatively, the molecular adsorption of oxygen on these nanotubes forms a bridge on a slanted B–C bond, creating a distorted square-like ring. From the binding energy calculations, the nanotubes are shown to be more reactive for atomic than for molecular oxygen. The obtained results for the binding energies prove that local ionization energy can be an appropriate indicator for monitoring the relative reactivity of boron and carbon atoms at SW defect region.

Calculation of the electronic properties of the perfect and defective BC_3 nanotubes shows that upon O_2 molecule adsorption, the semiconducting behavior of nanotubes is preserved in all cases, expect for SW-CC-c tube, which is a half-metallic antiferromagnet when adsorbs molecular oxygen. For perfect and SW-CC-a nanotubes, O_2 adsorbs without breaking the oxygen–oxygen bond and in line with this, no new state is created in the band gap. In other cases, new states appear below and/or above the Fermi level.

One aim of functionalizing nanotubes is to alter their electrical conductivity, especially for chemical sensors and nanobioelectronic devices. In this regard, the chemisorption of molecular oxygen is shown to reduce the band gap for the SW-BC-a system. In addition, the half-metallic antiferromagnet produced in the case of SW-CC-c/O_2 system is a novel material with potential applications in spintronics.

Acknowledgements

Computations were performed on the GPC supercomputer at the SciNet HPC Consortium. SciNet is funded by: the Canada Foundation for Innovation under the auspices of Compute Canada; the Government of Ontario; Ontario Research Fund – Research Excellence; and the University of Toronto.

References

[1] J. Zhao, A. Buldum, J. Han, J.P. Lu, Nanotechnology 13 (2002) 195.
[2] M. Arab, F. Picaud, M. Devel, C. Ramseyer, C. Girardet, Phys. Rev. B 69 (2004) 165401.
[3] J.V. Zanchetta, A. Marchand, Carbon 3 (1965) 332.
[4] W. Cermignani, T.E. Paulson, C. Onneby, C.G. Pantano, Carbon 33 (1995) 367.
[5] G.G. Fuentes, E. Borowiak-Palen, M. Knupfer, T. Pichler, J. Fink, L. Wirtz, A. Rubio, Phys. Rev. B 69 (2004) 245403.
[6] Y. Miyamoto, A. Rubio, S.G. Louie, M.L. Cohen, Phys. Rev. B 50 (1994) 18360.
[7] M.B. Nardelli, B.I. Yakobson, J. Bernholc, Phys. Rev. B 57 (1998) 4277.
[8] S. Jalili, M. Akhavan, J. Schofield, J. Phys. Chem. C 116 (2012) 13225.
[9] C. Wang, G. Zhou, H. Liu, J. Wu, Y. Qiu, B.-L. Gu, W. Duan, J. Phys. Chem. B 110 (2006) 10266.
[10] J. Andzelm, N. Govind, A. Maiti, Chem. Phys. Lett. 421 (2006) 58.
[11] M. Zhao, Y. Xia, J.P. Lewis, L. Mei, J. Phys. Chem. B 108 (2004) 9599.
[12] L.G. Zhou, S.Q. Shi, Appl. Phys. Lett. 83 (2003) 1222.
[13] B.C. Pan, W.S. Yang, J. Yang, Phys. Rev. B 62 (2000) 12652.
[14] X. Lu, Z. Chen, P.v.R. Schleyer, J. Am. Chem. Soc. 127 (2005,) 20.
[15] H.F. Bettinger, J. Phys. Chem. B 109 (2005) 6922.
[16] X.Y. Liu, W.G. Sun, C.Y. Wang, Y.J. Tang, Eur. Phys. J. D 56 (2010) 341.
[17] D. Vanderbilt, Phys. Rev. B 41 (1990) 7892.
[18] P. Giannozzi, S. Baroni, N. Bonini, M. Calandra, R. Car, C. Cavazzoni, D. Ceresoli, G.L. Chiarotti, M. Cococcioni, I. Dabo, et al., J. Phys. Condens. Matter 21 (2009) 395502.
[19] J.P. Perdew, K. Burke, M. Ernzerhof, Phys. Rev. Lett. 77 (1996) 3865.
[20] H.J. Monkhorst, J.D. Pack, Phys. Rev. B 13 (1976) 5188.
[21] T. Lu, F. Chen, J. Comput. Chem. 33 (2012) 580.
[22] M.J. Frisch, G.W. Trucks, H.B. Schlegal, G.E. Scuseria, M.A. Robb, J.C. Cheeseman, J.M. Millam, S.S. Lyengar, J. Tomasi, V. Barone, et al., Gaussian 03, revision C.02, Gaussian Inc, Wallingford, CT, 2004.
[23] W. Humphrey, A. Dalke, K. Schulten, J. Mol. Graphics 14 (1996) 33.
[24] Y.-H. Kim, H.-S. Sim, K.J. Chang, Curr. Appl. Phys. 1 (2001) 39.
[25] S. Picozzi, S. Santucci, L. Lozzi, L. Valentini, B. Delley, J. Chem. Phys. 120 (2004) 7147.
[26] Y. Li, Z. Zhou, G. Dmitri, Y. Bando, P.v.R. Schleyer, C. Zhongfang, J. Phys. Chem. C 112 (2008) 1365.
[27] S. Jalili, M. Akhavan, J. Schofield, Mol. Phys. 111 (2013) 888.
[28] W. An, X. Wu, J.L. Yang, X.C. Zeng, J. Phys. Chem. C 111 (2007) 14105.
[29] D.C. Sorescu, K.D. Jordan, P. Avouris, J. Phys. Chem. B 105 (2001) 11227.
[30] P. Politzer, J.S. Murray, F.A. Bulat, J. Mol. Model. 16 (2010) 1731.
[31] P. Giannozzi, R. Car, G. Scoles, J. Chem. Phys. 118 (2003) 1003.
[32] S. Dag, O. Gülseren, T. Yildirim, S. Ciraci, Phys. Rev. B 67 (2003) 165424.
[33] Y. Chen, C.-L. Hu, J.-Q. Li, G.-X. Jia, Y.-F. Zhang, Chem. Phys. Lett. 449 (2007) 149.
[34] B. Shan, K. Cho, Chem. Phys. Lett. 492 (2010) 131.
[35] M. Grujicic, G. Cao, A.M. Rao, T.M. Tritt, S. Nayak, Appl. Surf. Sci. 214 (2003) 289.
[36] R.E. Rudd, W.E. Pickett, Phys. Rev. B 57 (1998) 557.
[37] X. Hu, Adv. Mater. 24 (2012) 294.